



Uncertainty propagation through an aeroelastic wind turbine model using polynomial surrogates

Murcia Leon, Juan Pablo; Réthoré, Pierre-Elouan Mikael; Dimitrov, Nikolay Krasimirov; Natarajan, Anand; Sørensen, John Dalsgaard; Graf, Peter; Kim, Taeseong

Published in:
Renewable Energy

DOI (link to publication from Publisher):
[10.1016/j.renene.2017.07.070](https://doi.org/10.1016/j.renene.2017.07.070)

Creative Commons License
CC BY-NC-ND 4.0

Publication date:
2018

Document Version
Accepted author manuscript, peer reviewed version

[Link to publication from Aalborg University](#)

Citation for published version (APA):
Murcia Leon, J. P., Réthoré, P.-E. M., Dimitrov, N. K., Natarajan, A., Sørensen, J. D., Graf, P., & Kim, T. (2018). Uncertainty propagation through an aeroelastic wind turbine model using polynomial surrogates. *Renewable Energy*, 119, 910-922. <https://doi.org/10.1016/j.renene.2017.07.070>

General rights

Copyright and moral rights for the publications made accessible in the public portal are retained by the authors and/or other copyright owners and it is a condition of accessing publications that users recognise and abide by the legal requirements associated with these rights.

- Users may download and print one copy of any publication from the public portal for the purpose of private study or research.
- You may not further distribute the material or use it for any profit-making activity or commercial gain
- You may freely distribute the URL identifying the publication in the public portal -

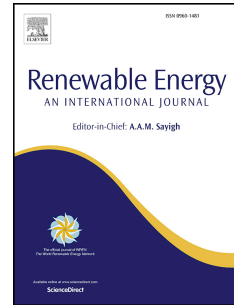
Take down policy

If you believe that this document breaches copyright please contact us at vbn@aub.aau.dk providing details, and we will remove access to the work immediately and investigate your claim.

Accepted Manuscript

Uncertainty propagation through an aeroelastic wind turbine model using polynomial surrogates

Juan Pablo Murcia, Pierre-Elouan Réthoré, Nikolay Dimitrov, Anand Natarajan, John Dalsgaard Sørensen, Peter Graf, Taeseong Kim



PII: S0960-1481(17)30698-5

DOI: [10.1016/j.renene.2017.07.070](https://doi.org/10.1016/j.renene.2017.07.070)

Reference: RENE 9045

To appear in: *Renewable Energy*

Received Date: 27 September 2016

Revised Date: 17 April 2017

Accepted Date: 14 July 2017

Please cite this article as: Murcia JP, Réthoré P-E, Dimitrov N, Natarajan A, Sørensen JD, Graf P, Kim T, Uncertainty propagation through an aeroelastic wind turbine model using polynomial surrogates, *Renewable Energy* (2017), doi: 10.1016/j.renene.2017.07.070.

This is a PDF file of an unedited manuscript that has been accepted for publication. As a service to our customers we are providing this early version of the manuscript. The manuscript will undergo copyediting, typesetting, and review of the resulting proof before it is published in its final form. Please note that during the production process errors may be discovered which could affect the content, and all legal disclaimers that apply to the journal pertain.

Uncertainty propagation through an aeroelastic wind turbine model using polynomial surrogates

Juan Pablo Murcia^a, Pierre-Elouan Réthoré^b, Nikolay Dimitrov^b, Anand Natarajan^b,
John Dalsgaard Sørensen^{b,c}, Peter Graf^d, Taeseong Kim^b

^a*jumu@dtu.dk, Department of Wind Energy, Technical University of Denmark.
Risø Campus, Frederiksborgvej 399 Building 125. 4000 Roskilde. Denmark*

^b*Department of Wind Energy, Technical University of Denmark*

^c*Department of Civil Engineering, Aalborg University*

^d*National Renewable Energy Laboratory, Colorado USA*

Abstract

Polynomial surrogates are used to characterize the energy production and lifetime equivalent fatigue loads for different components of the DTU 10 MW reference wind turbine under realistic atmospheric conditions. The variability caused by different turbulent inflow fields are captured by creating independent surrogates for the mean and standard deviation of each output with respect to the inflow realizations. A global sensitivity analysis shows that the turbulent inflow realization has a bigger impact on the total distribution of equivalent fatigue loads than the shear coefficient or yaw misalignment. The methodology presented extends the deterministic power and thrust coefficient curves to uncertainty models and adds new variables like damage equivalent fatigue loads in different components of the turbine. These surrogate models can then be implemented inside other work-flows such as: estimation of the uncertainty in annual energy production due to wind resource variability and/or robust wind power plant layout optimization. It can be concluded that it is possible to capture the global behavior of a modern wind turbine and its uncertainty under realistic inflow conditions using polynomial response surfaces. The surrogates are a way to obtain power and load estimation under site specific characteristics without sharing the proprietary aeroelastic design.

Keywords: Wind energy, uncertainty quantification, aeroelastic wind turbine model, annual energy production, lifetime equivalent fatigue loads

1. Introduction

2 The wind turbine design standard IEC 61400-1 [1] provides wind climate specifica-
3 tions which are used as a reference for the structural design of the wind turbines. For
4 achieving type certification of a new turbine model, the designer has to demonstrate
5 that the structural capacity of the turbine is sufficient for withstanding the reference

6 wind conditions over the entire lifetime of the turbine. Such a demonstration is nor-
7 mally given by dynamic load simulations which characterize the behavior of the turbine
8 under the reference wind conditions. Once certification is achieved, the given turbine
9 model can safely be installed on sites where the wind conditions are identical or more
10 benign than the reference standard conditions. However, in many occasions one or
11 more of the parameters describing the site environmental conditions will be outside
12 the ranges which are sufficiently covered by the IEC reference conditions. In such
13 cases, it is necessary to estimate the actual loads which the turbine will experience
14 over its entire lifetime, by considering the full joint distribution of the variables that
15 describe the turbulent inflow. This is similar to a propagation of uncertainty prob-
16 lem in which the distribution of the atmospheric conditions on the site needs to be
17 propagated through the aeroelastic model of the turbine.

18 If a full design load case setup similar to the IEC 61400-1 design cases is used for that
19 purpose, the problem quickly becomes time-consuming as new dynamic simulations
20 would be required for each site. As an example, the number of simulations required to
21 predict within 1% error the lifetime equivalent fatigue loads on a floating wind turbine
22 where the inflow conditions (sea/wind) are characterized by five stochastic variables
23 can reach up to $3,200,000 = 20^5$ using regular grid-based estimates or in the order
24 of 50,000 using Monte-Carlo (MC) simulation [2]. An approach that alleviates these
25 issues is mapping the turbine response to different environmental inputs by means of
26 a fast and accurate surrogate model. Several techniques can be used to predict the
27 behavior of the turbine from a limited set of model evaluations such as: interpolation
28 techniques, response surface techniques [3], Gaussian process (Kriging) [4] and machine
29 learning techniques [5, 6].

30 Polynomial chaos expansion is a methodology used to efficiently propagate input
31 uncertainties through a non-linear model. This methodology consists in building a
32 polynomial response surface to capture the global dependency of the output as a func-
33 tion of the uncertain inputs. PCE is widely used in the uncertainty quantification field
34 because of its simplicity and fast convergence in comparison to a full MC simulation
35 based on the original model [7, 8, 9, 10, 11]. Furthermore, adaptive PCE training al-
36 gorithms can be used to obtain a sparse surrogate that minimizes the number of terms
37 that have multiple variable dependency, making the surrogates extremely efficient re-
38 sponse surfaces in multiple dimensions [12, 13, 14]. In the case of smooth continuous
39 models with multiple input variables, sparse polynomial chaos expansion methodology
40 is the most efficient technique to build the surrogates in terms of the number of model
41 evaluations required, the number of input dimensions they can handle and the rate of
42 convergence [12].

43 One of the main difficulties in building a surrogate of an aeroelastic wind turbine
44 model is the fact that the turbulent inflow realization (TIR, i.e. turbulent structures
45 in the flow field) causes variations in the different wind turbine model outputs: such
46 as power, thrust, fatigue and extreme loads in the different components of the tur-
47 bine. This can be restated as: an aeroelastic wind turbine model has stochastic/non-
48 deterministic outputs. Many studies have analyzed the difficulties of studying fatigue

49 and extreme loads under different turbulent inflow realizations [15, 16, 17, 4, 3]. Differ-
 50 ent TIR activate different dynamics of the structure and have different control system
 51 responses; therefore are an important source of uncertainty in the prediction of the
 52 outputs of the model [15]. The high variability in the model response to certain tur-
 53 bulent inflow structures has also been shown to be problematic when MC simulation
 54 was used to predict lifetime averages of fatigue loads on a floating wind turbine [2].

55 1.1. Response to the problem

56 The aim of the present study is to demonstrate a method for building a quick and
 57 accurate surrogate of a wind turbine model that predicts the turbine response as a
 58 function of multiple stochastic input variables that describe the turbulent inflow on
 59 a site (\mathbf{x}). The surrogate for the turbine model is a set of two independent sparse
 60 polynomial response surfaces that allow to predict the variability caused by different
 61 input variable distributions and by different turbulent inflow field realizations (TIR).
 62 One response surface characterizes the expected output with respect to TIR: $\hat{y}_{\mathbb{E}}(\mathbf{x}) \approx$
 63 $\mathbb{E}_{\text{TIR}}(y|\mathbf{x})$. The other one describes the standard deviation of the output with respect
 64 TIR: $\hat{y}_{\mathbb{S}}(\mathbf{x}) \approx \sqrt{\mathbb{V}_{\text{TIR}}(y|\mathbf{x})}$; which is a model that predicts the uncertainty in the
 65 turbine response due to different turbulent structures hitting the turbine. Finally, a
 66 sample can be obtained from the normal distribution constructed using the mean and
 67 the standard deviation surrogates in order to make a prediction of the variability in
 68 the output at a given input point:

$$\hat{y}(\mathbf{x}) \sim \text{Normal}(\hat{y}_{\mathbb{E}}(\mathbf{x}), \hat{y}_{\mathbb{S}}(\mathbf{x})) \quad (1)$$

69 The final surrogate $\hat{y}(\mathbf{x})$ can then be used to obtain distributions of the wind turbine
 70 power and fatigue loads in a given year whose input parameters (wind, wind/sea, or
 71 wind/geological conditions) follow the distribution used to train the surrogate PDF(\mathbf{x}).
 72 Since the surrogate is a response surface it can also be used to predict the distribution
 73 of the outputs when the input distributions is close but not exactly the distribution
 74 used for training the surrogate. This setup is considered a multi-leveled uncertainty
 75 propagation and it is the scenario that occurs when there is uncertainty in the param-
 76 eters that characterize the WS distribution for example. This approach is necessary to
 77 estimate the uncertainty in annual energy production and lifetime averaged equivalent
 78 fatigue load.

79 1.2. Article overview

80 A general overview of the PCE methodology in multiple dimensions is presented in
 81 section 2. This section describes the Rosenblatt transformation, the design of experi-
 82 ments used to define the training simulation points, the approach used to train sparse
 83 polynomial response surfaces and the logistic transformation used to limit the output.
 84 In section 3, the methodology is then applied to the response of the DTU 10 MW ref-
 85 erence wind turbine HAWC2 model [18] to turbulent inflow fields characterized by four
 86 input parameters. The four input parameters are the 10-min averaged hub height wind

87 speed (WS), the turbulent standard deviation of the instantaneous wind speed in the
 88 streamwise component (σ_1), the shear exponent (α) and the yaw misalignment angle
 89 (γ). A study of how many independent realizations of the turbulent inflow field are
 90 required to achieve a certain error tolerance in the surrogate is presented in the section
 91 3.7. Finally in section 3.8, the surrogates are used in an example of prediction of the
 92 uncertainty in the annual energy production and the uncertainty in lifetime averaged
 93 equivalent fatigue loads.

94 2. Methods

95 This article proposes the use of two different variable transformations to simplify
 96 the polynomial response surface fitting problem, see figure 1. The first transforma-
 97 tion is the Rosenblatt transformation [19], which is used to de-correlate the set of
 98 D input variables $\mathbf{x} = (x_0, x_1, \dots, x_{D-1})$ into a set of independent uniform variables,
 99 $\mathbf{w} = (w_0, w_1, \dots, w_{D-1})$. The second transformation is a logistic transformation, and it
 100 is used to enforce constraints on the polynomial surrogates [20]. This transformation
 101 enables the use of polynomial surrogates in problems where the output has a minimum
 102 and/or maximum value. Without the logistic transformation the polynomial surrogates
 103 will present oscillations in the regions where the model has a constant output. The
 104 power production of a turbine is an example of a variable with a strict upper constraint
 105 corresponding to the rated power.

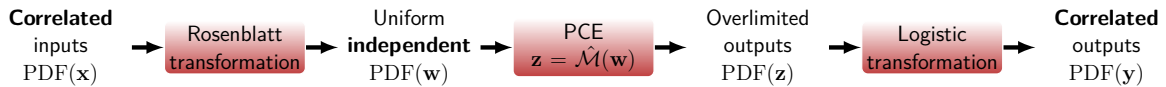


Figure 1: Transformation of variables to build efficient polynomial response surface.

106 2.1. 1D PCE theory

107 Consider a model with a single uncertain input (x) and a single output (y). PCE
 108 consists of defining a polynomial family that is orthogonal with respect to the input
 109 distribution, PDF(x). Orthogonal polynomial families with respect to the most im-
 110 portant distributions are well known, see table 1. For details on how to define new
 111 polynomial basis to an arbitrary input distributions refer to Gautschi et al [21].

Distribution	Polynomial Family
Uniform	Legendre
Normal	Hermite
Exponential	Laguerre

Table 1: Classical orthogonal polynomial families.

112 The orthogonal polynomials are used to build a polynomial approximation of the
 113 output, i.e. a polynomial response surface, see equation 2. Where, $\phi_l(x)$ is the l

114 order orthogonal polynomial, c_l is its correspondent coefficient and M represents the
 115 truncation order of the PCE.

$$y(x) \approx \hat{y}(x) = \sum_{l=0}^M c_l \phi_l(x) \quad (2)$$

116 There are two different approaches to determine the c_l coefficients:

117 *Semi-Spectral projection* consists in using quadrature rules to approximate the in-
 118 ner product definition of the coefficient, see equation 3. Many quadrature rules exist
 119 to approximate the integrals; but all quadrature rules give N_n nodes for model evalu-
 120 ation (x_i) and their corresponding weights (ω_i). Gaussian quadrature rules are widely
 121 used because they are accurate for smooth function integration with respect a weight
 122 function, in this case the PDF(x), see equation 3.

$$c_l = \langle y, \phi_l \rangle \equiv \int y(x) \phi_l(x) \text{PDF}(x) dx \approx \sum_{i=0}^{N_n} \omega_i y(x_i) \phi_l(x_i) \quad (3)$$

123 In general, semi-spectral projection is an efficient method for low number of input
 124 dimensions, but the number of model evaluations required grows exponentially with
 125 the number of dimensions. Additionally, quadrature rules can be unstable for heavy
 126 tailed PDFs such as the Weibull distribution [21].

127 *Point collocation* consists in fitting the polynomial basis to a small sample of model
 128 evaluations. Traditionally, this fit can be done using least squares algorithm, but some
 129 other optimization algorithms can be used to obtain PCE approximations that mini-
 130 mize the number of terms in the surrogate [12, 13, 14]. This techniques are explained in
 131 the section 2.5. In general, point collocation is robust and the advanced optimization
 132 algorithms are designed to handle large number of dimensions, to avoid over-fitting
 133 and to achieve sparsity in the final surrogate. The present study focuses only in the
 134 point collocation techniques since the number of model evaluations required to fit a
 135 multiple dimensional PCE is smaller [12] than in other methods.

136 2.2. Rosenblatt transformation

137 To build the PCE of a model with multiple correlated inputs (\mathbf{x}), it is required to
 138 initially transform the correlated input space into an uncorrelated space ($\mathbf{w} = R^{-1}(\mathbf{x})$).
 139 In this article, the Rosenblatt transformation is used because the input distribution of
 140 the turbulent inflow field parameters are usually defined in a sequence of conditional
 141 relationships [19]. Refer to Dimitrov et al [22] and Graf et al [2] for examples of
 142 such distributions used for offshore and floating wind turbine fatigue and extreme load
 143 analysis.

144 Since all the variables are transformed into uncorrelated unitary uniform variables
 145 then the PCE only requires the use of the Legendre polynomials: $y(\mathbf{x}) = y(R(\mathbf{w})) \approx$
 146 $\hat{y}(\mathbf{w})$.

147 *2.3. Multi-dimensional PCE*

148 A D -dimensional polynomial is constructed as the sum of the product between
 149 individual one dimensional polynomials for each of the D uniform input variables,
 150 $\mathbf{w} = [w_0, \dots, w_{D-1}]$. The D -dimensional surrogate is written using a set of multiple
 151 indexes $\mathcal{I} \subset \mathbb{N}^D$. An element $J \in \mathcal{I}$ contains the order of the polynomial in each
 152 dimension: $J = [l_0, \dots, l_{D-1}]$. Additionally, the multiple indexes are enumerated,
 153 $J \leftrightarrow j \in \mathbb{N}$. A surrogate that contains N_c terms can be written as:

$$y(\mathbf{x}) = y(R(\mathbf{w})) \approx \sum_{j=0}^{N_c-1} c_j \phi_j(\mathbf{w}) \quad (4)$$

154 where an element in the multidimensional polynomial basis is given as:

$$\phi_j(\mathbf{w}) = \phi_{l_0}(w_0) \times \dots \times \phi_{l_{D-1}}(w_{D-1}) \quad (5)$$

155 *2.4. Training point selection*

156 The Rosenblatt transformation enables the use of multiple variance reduction MC
 157 sampling techniques to define the training points of a surrogate [23]. Latin hypercube
 158 sampling [24], Sobol sequence [25] and Hammersley sequence [26] are some examples of
 159 such techniques. These techniques are designed to sample from the unitary hypercube
 160 of D dimensions, i.e. the uniform distributed variables: $\mathbf{w}_i \sim \text{PDF}(\mathbf{w})$. Finally, the
 161 Rosenblatt transformation is used to transform each realization in the uniform sample
 162 into the correlated input space, $\mathbf{x}_i = R(\mathbf{w}_i) \sim \text{PDF}(\mathbf{x})$.

163 The number of unknown coefficients c_j in a D -dimensional PCE depends of the
 164 total polynomial order of the PCE. The total order is defined as the maximum sum
 165 of the one dimensional orders. If the PCE is truncated to a total order M then the
 166 number of unknown coefficients is given by the following combination:

$$N_c = \binom{M+D}{M} = \frac{(M+D)!}{M! D!} \quad (6)$$

167 The number of model evaluations should be between 2 or 3 times the number of
 168 unknowns in order to have extra data to test the accuracy of the surrogate and to
 169 implement strategies to avoid over-fitting [12]. Note that the maximum order is only
 170 used to estimate the number of model evaluations. Advanced regression techniques
 171 allow to explore higher order terms [14, 12]. The maximum order M can be increased
 172 in order to achieve higher accuracy surrogates but at the cost of having more model
 173 evaluations and the requirement of assuring that there is no over-fitting.

174 *2.5. Point collocation and the LASSO problem*

175 The least absolute shrinkage and selection operator (LASSO) problem is a modified
 176 least squares optimization problem that adds a term that penalizes the amount of active
 177 terms in the surrogate (terms with non zero coefficients). LASSO is used to achieve
 178 sparsity and to avoid over fitting in the polynomial surrogate. Additionally, the number

179 of model evaluations required for solving the LASSO problem is smaller in comparison
 180 to a least squares regression that has the same maximum total polynomial order [12].

181 A LASSO problem can be described as finding the set of coefficients c_j that mini-
 182 mizes the sum of squared errors plus the sum of the absolute values of all coefficients
 183 (ℓ_1 norm regularization term) [14]:

$$\min_{c_j} \sum_{i=0}^{N-1} \left[\sum_{j=0}^{N_c-1} c_j \phi_j(\mathbf{w}_i) - y(\mathbf{x}_i) \right]^2 + \alpha \sum_{j=0}^{N_c-1} |c_j| \quad (7)$$

184 where the number of model/surrogate evaluation points N is fixed. Note that the
 185 input and surrogate evaluation points are related by the Rosenblatt transformation
 186 $\mathbf{x}_i = R(\mathbf{w}_i)$. The maximum number of possible terms of the surrogate N_c is fixed by
 187 selecting a maximum total multi-dimensional polynomial order.

188 The regularization coefficient α controls the amount of active terms in the final
 189 solution. Smaller values allow to have more active terms while larger values will prefer
 190 final surrogates with few active terms. A sparse surrogate has the advantage of making
 191 the evaluation of the multi-dimensional surrogate faster in comparison to the full least
 192 squares solution; this advantage becomes critical in high number of input dimensions.

193 There are two algorithms widely used to solve the LASSO problem: coordinate
 194 descent [14] and least angle regression (LAR) [12]. Coordinate decent is used in the
 195 present work because it tends to be more stable for high dimensional problems [13]. The
 196 reason for this is that coordinate descent operates on a given regularization coefficient
 197 instead of exploring the full space of α 's as in LAR algorithm.

198 Cross-validation is used to select the regularization coefficient α that minimizes
 199 over fitting of the data. A k-fold cross-validation consists in splitting the dataset into
 200 k groups of data. All the points in k-1 groups are used for training and the remaining
 201 group is used for cross-validation. This means that the surrogate fitted using k-1
 202 groups is used to predict the output in each of the elements of the remaining group.
 203 The mean squared error of the prediction of the surrogate is then computed. This
 204 process is repeated leaving out each individual fold and for multiple regularization
 205 parameters. The regularization parameter that gives the lowest mean cross-validation
 206 mean squared errors is then selected to train the whole dataset. This translates as
 207 selecting the sparse model that performs the best by predicting missing data, i.e. that
 208 has less over-fitting.

209 2.6. Logistic transformation

210 A logistic transformation is applied to an output of the model in order to avoid
 211 oscillations in the regions where the model is constant. In practice this transformation
 212 is used to impose strict restrictions on the polynomial surrogates. The transformation
 213 consists in applying the *logit* function, $L(p) = \ln\left(\frac{p}{1-p}\right)$, to the model output at the
 214 training points $y_i = y(\mathbf{x}_i)$ into the over-shooting variable space: $z_i = L(a_1 y_i + a_0)$
 215 [20]. Finally, each time the surrogate is evaluated, the prediction of the surrogate is

216 transformed back to the original output space $\hat{y} = (L^{-1}(\hat{z}) - a_0)/a_1$. The constants of
 217 the transformation are calibrated in order to impose the constraints of the output and
 218 to avoid numerical instabilities that are inherent to the logit function.

219 2.7. Global sensitivity analysis

220 Global sensitivity analysis (SA) is a methodology to determine how important each
 221 input is to explain the variance of the output. SA can be obtained with a Sobol variance
 222 decomposition [27]. In this technique, the variance of the output is explained into the
 223 different terms of variance of each of the inputs, in a process similar to the analysis
 224 of the variance of experiments (ANOVA) [28]. Total effect Sobol indices are widely
 225 used as measures of how much of the variance of a given output is explained by the
 226 variance of an input, including possible interactions with other variables. This method
 227 is the most recognized method for global sensitivity analysis because it accounts for
 228 non-linear dependencies and for interactions between variables [29].

229 Variance decomposition can be expressed as the sum of the variance of the marginal
 230 expected value of a subset of input variables, see equation 8. Note that this decom-
 231 position is not an infinite series expansion, it is truncated to the maximum number of
 232 variable interactions.

$$\begin{aligned} \mathbb{V}(y) &= \sum_{k=0}^{D-1} \mathbb{V}_k + \sum_{k=0}^{D-1} \sum_{l>k}^{D-1} \mathbb{V}_{kl} + \sum_{k=0}^{D-1} \sum_{l>k}^{D-1} \sum_{m>l}^{D-1} \mathbb{V}_{klm} + \dots + \mathbb{V}_{0\dots D-1} \\ \mathbb{V}_k &= \mathbb{V}(\mathbb{E}_{\forall n \neq k}(\mathcal{M}(\mathbf{x}|x_k))) \\ \mathbb{V}_{kl} &= \mathbb{V}(\mathbb{E}_{\forall n \neq k,l}(\mathcal{M}(\mathbf{x}|x_k, x_l))) \\ \mathbb{V}_{klm} &= \mathbb{V}(\mathbb{E}_{\forall n \neq k,l,m}(\mathcal{M}(\mathbf{x}|x_k, x_l, x_m))) \end{aligned} \quad (8)$$

233 The global sensitivity measure is defined by normalizing eq. 8 with the total vari-
 234 ance of the output $\mathbb{V}(y)$. From this normalization one can define the Sobol index of a
 235 given degree of interaction between input variables as:

$$S_k = \frac{\mathbb{V}_k}{\mathbb{V}(y)} \quad S_{kl} = \frac{\mathbb{V}_{kl}}{\mathbb{V}(y)} \quad S_{klm} = \frac{\mathbb{V}_{klm}}{\mathbb{V}(y)} \quad \dots \quad (9)$$

236 The total effect Sobol index of an input variable x_i is then the sum of all the Sobol
 237 indices that include the variable in any interaction:

$$S_{\text{total } x_i} = S_i + \sum_{\substack{k=0 \\ k \neq i}}^{D-1} S_{ik} + \dots \quad (10)$$

238 The sensitivity analysis of the response of the turbine should consider the effect
 239 of having different turbulent inflow realizations which is modeled with the two inde-
 240 pendent polynomial response surfaces for the local mean and local standard deviation.
 241 The Sobol indexes are not computed directly from the PCE coefficients as for classi-
 242 cal problems, see Sudret et al [30], because the Logistic transformation removes the

243 stochastic properties of the PCE and because the coefficients of the local mean sur-
 244 rogate would not include the effect of the turbulence inflow realization. To solve this
 245 limitation, the approximate method proposed in Saltelli et. al [29] is used to compute
 246 the total effect Sobol indexes. This approach estimates the total effect Sobol indexes
 247 from a large MC simulation.

248 3. Results

249 3.1. Implementation

250 Several open source implementations of PCE methods are available such as: Chaospy
 251 [23], Dakota [31], UQLab [32] and OpenTurns [33]. In the present work we use Chaospy
 252 because of its implementation of the Rosenblatt transformation. Additionally, the
 253 present work uses the LASSO problem solvers [14] and the cross-validation capabilities
 254 available in the open source library Scikit-learn [13]. These capabilities are used in-
 255 side of Chaospy for general users and are used externally in the present study to gain
 256 control over the different stages of the cross-validation.

257 3.2. Case description

258 The model consists of the DTU 10 MW reference wind turbine HAWC2 model
 259 [34, 18] with Mann turbulent inflow generation [35]. The turbulent inflow conditions
 260 are defined using the four variables described in table 2.

Input	Variable	Distribution	Parameters	
10-min mean hub height wind speed	$x_0 = \text{WS}$	Rayleigh	$\mathbb{E}(\text{WS}) = 10 \text{ m/s}$	
Std. of the inst. wind speed in the streamwise direction during the 10-min simulation	$x_1 = \sigma_1$	Lognormal	$\mu_{\sigma_1}(\text{WS})$	$\sigma_{\sigma_1}(\text{WS})$
10-min mean shear exponent	$x_2 = \alpha$	Normal	$\mu_{\alpha}(\text{WS})$	$\sigma_{\alpha}(\text{WS})$
10-min mean yaw miss-align.	$x_3 = \gamma$	Normal	$\mu_{\gamma} = 0$	$\sigma_{\gamma} = 5 \text{ deg.}$

Table 2: Wind turbine model inputs.

261 The dependency between WS and σ_1 is defined in the Normal Turbulence Model
 262 described in the IEC 61400-1 [1]. The present case uses a reference ambient turbulence
 263 intensity of a site Class 1A: $\text{TI}_{\text{ref}} = 0.16$. This dependency is given by the local statisti-
 264 cal moments of σ_1 as: $\mathbb{E}(\sigma_1|\text{WS}) = \text{TI}_{\text{ref}}(0.75\text{WS} + 3.8)$ and $\mathbb{V}(\sigma_1|\text{WS}) = (1.4 \text{TI}_{\text{ref}})^2$.

265 The parameters of the σ_1 distribution are given in equation 11 as functions of WS.

$$\sigma_{\sigma_1} = \left(\ln \left(\frac{\mathbb{V}(\sigma_1|\text{WS})}{\mathbb{E}^2(\sigma_1|\text{WS})} + 1 \right) \right)^{1/2} = \left(\ln \left(\frac{1.4^2}{(0.75\text{WS} + 3.8)^2} + 1 \right) \right)^{1/2} \quad (11)$$

$$\mu_{\sigma_1} = \ln(\mathbb{E}(\sigma_1|\text{WS})) - \frac{\sigma_{\sigma_1}^2}{2} = \ln(\text{TI}_{\text{ref}}(0.75\text{WS} + 3.8)) - \frac{\sigma_{\sigma_1}^2}{2}$$

266 The correlation between α and WS is based on the simplified joint distribution
 267 defined by Dimitrov et al [22]:

$$\begin{aligned}\mu_\alpha &= 0.088(\ln(\text{WS}) - 1) \\ \sigma_\alpha &= 1/\text{WS}\end{aligned}\quad (12)$$

268 Seven different model outputs are considered (\mathbf{y}), see table 3. The damage equiva-
 269 lent fatigue loads (EFL) are computed using a rainflow counting algorithm to determine
 270 the number of load cycles n_i with their corresponding load range S_i in the 10-min time
 271 series of turbine response. The EFL is then obtained using different materials' Wöhler
 272 exponent m , see equation 13 [36]. For obtaining 1Hz-equivalent fatigue loads based on
 273 10 minute reference periods, the reference number of load cycles used is $N_{\text{ref}} = 600$.

$$S_{\text{eq}} = \left(\frac{\sum n_i S_i^m}{N_{\text{ref}}} \right)^{\frac{1}{m}} \quad (13)$$

Output	m	Variable
10 minute mean power production	-	P
10 minute mean thrust coefficient	-	CT
EFL blade root flapwise bending moment	12	BRF
EFL tower bottom fore-aft bending moment	4	TBF
EFL tower bottom sidewise bending moment	4	TBS
EFL tower top tilt bending moment	4	TTT
EFL tower top yaw bending moment	4	TTY

Table 3: Wind turbine model outputs.

274 3.3. Training points

275 In this study, the number of model evaluations are set to be $N = 2N_c$, the max-
 276 imum order of the polynomial is expected to be $M = 4$ and the number of input
 277 variables is $D = 4$. This leads to 140 total number of model evaluations, i.e. 140 input
 278 variables locations for which HAWC2 model is executed, see equation 6. A Ham-
 279 mersley sequence [26] is preferred over other variance reduction methods to generate the
 280 training sample in the uniform space as it is a sequence that can be extended to contain
 281 larger sample size without changing the previous points [23, 37]. The uniform sample
 282 is then transformed into the physical variables using the Rosenblat transformation. A
 283 similar approach is used to generate the input sample for a MC simulation on either
 284 the real model or the surrogate models; the size of the MC sample is taken to be 80000.
 285 The training input sample is shown in figure 2 as well as a the inputs sample for the
 286 MC simulation. figure 2 is a representation of the multidimensional PDF(\mathbf{x}): the his-
 287 tograms represent the marginal distributions for each variable, while the plots in the
 288 lower diagonal represent the training points and bi-dimensional histograms of the MC
 289 sample. The figures in the lower diagonal show the correlations between each pairs of
 290 variables as well as the iso-pdf quantiles that enclose 68%, 95% and 99.7% of the data.

291 It can be observed that the training points are more densely distributed in the regions
 292 of higher probability of the inputs. This means that the surrogate is better trained
 293 in the most likely region of the input space. For applications where the quantity of
 294 interest is the tail of the output distribution, such as ultimate load estimation, the
 295 training dataset could be distributed uniformly over the region encircled by a given
 296 iso-pdf quantile of the inputs, see iso-PDF contours in figure 2. 100 different turbulent
 297 inflow realizations are generated using the Mann model for each input point, for which
 298 the mean and standard deviation of the outputs are obtained. This number is selected
 299 to test the accuracy of the prediction of the surrogates when they are trained using a
 300 reduced number of TIR as it is defined in the design load cases defined in the standard
 301 [1]. The full training sample consists of 140×100 HAWC2 10 minutes simulations.

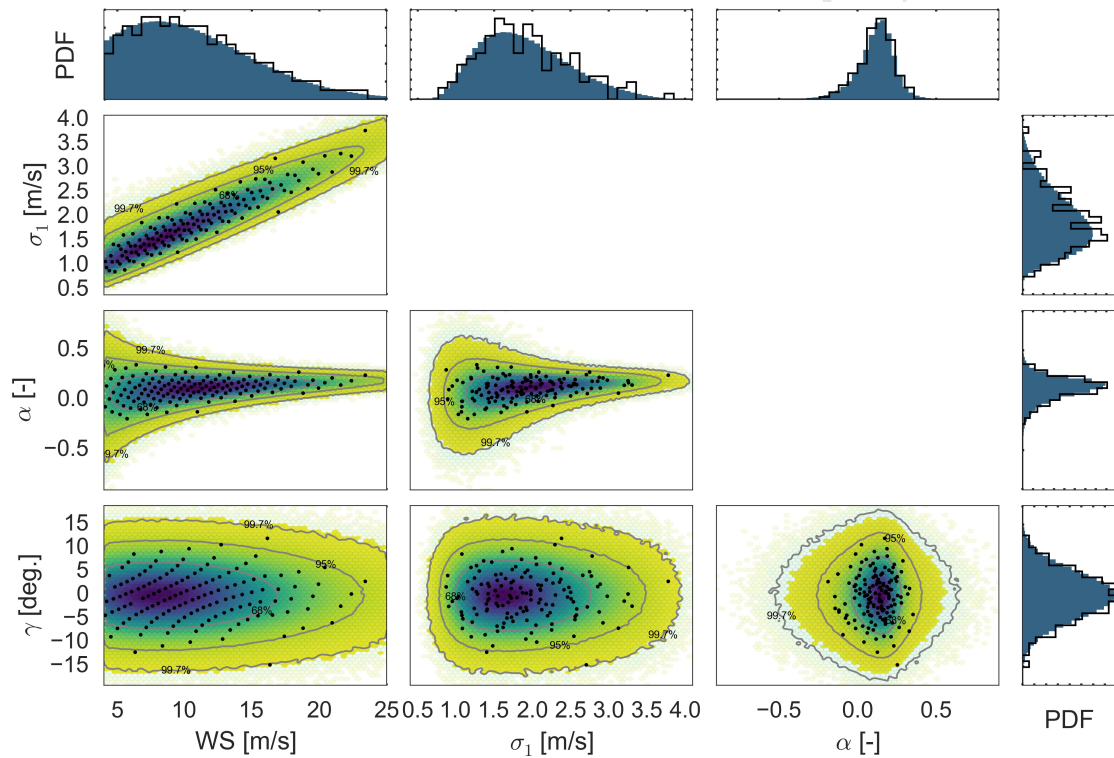


Figure 2: (Black points) Training dataset in the inputs: 140 Hammersley sequence sample of input joint distribution. (Histogram colored hex-bins) 80000 Hammersley sequence MC sample. (Contour lines) Iso-PDF lines that encircle 68%, 95% and 99.7% of the MC sample.

3.4. Example of PCE surrogates for individual statistical moments

302 Some examples of the distribution of $\mathbf{y}_{\mathbb{E}}$ and $\mathbf{y}_{\mathbb{S}}$ ¹ are shown in figure 3. In this
 303 figure the black points represent the observed statistic of the output for the training
 304

¹ $P_{\mathbb{S}}$ represents the standard deviation of 100 different realizations of the 10-min averaged power; this variable should not be confused with the standard deviation of the instantaneous power during the 10 minutes of simulation.

305 points; while the bi-dimensional histogram represents the obtained distribution of the
 306 surrogate for a 80000 MC sample. The observed histogram in the training dataset and
 307 the PDF predicted by the surrogate for \mathbf{y}_E and \mathbf{y}_S are shown in the last column in
 308 figure 3. It can be observed that the surrogates accurately capture the global PDF of
 309 the model and its dependency with respect to the 4 input variables. The surrogates of
 310 the local standard deviations, \hat{y}_S , are not able to capture the behavior of some extreme
 311 cases, see the extreme points at low wind speeds in the plots for CT_S and BRF_S . These
 312 errors are small in comparison to the overall magnitude of the output; the distribution
 313 of the errors of the surrogates and its impact in the final prediction are quantified in
 314 section 3.7. These errors can be reduced up to a tolerance level selected by the user
 315 by adding more training points (input points with their turbulent inflow realizations).
 316 The surrogates are robust enough to predict the frequency of occurrence of extreme
 317 values such as the outputs resulting from the input point with largest σ_1 , see first and
 318 third row in figure 3. This point seems to be outside the main trend in WS in figure 3
 319 because it has a large σ_1 and α given its WS, see figure 2.

320 3.5. Final surrogate predictions

321 The surrogates of \mathbf{y}_E and \mathbf{y}_S are combined to estimate the distribution of each indi-
 322 vidual output of the DTU 10 MW RWT. The prediction is done by sampling the normal
 323 distribution constructed using the surrogates of \mathbf{y}_E and \mathbf{y}_S , see equation 1. These re-
 324 sults are presented in figure 4 along with the full dataset of HAWC2 simulations. In
 325 this figure each cross represents an individual 10-min simulation, therefore the scatter
 326 of nearby simulations illustrates the stochasticity in the output of the aeroelastic sim-
 327 ulation. The amount of local output variability due to the turbulent inflow realization
 328 varies between outputs and depends on the region of the input space. The effect of the
 329 turbulent inflow realization is more important for the fatigue loads than for power and
 330 thrust coefficient. figure 4 also presents the bi-dimensional histogram obtained with
 331 a 80000 MC simulation of the surrogate. The distribution predicted by the surrogate
 332 captures the dependency and variability of each output with respect to the four input
 333 variables; the iso-PDF quantiles that encircle the 68%, 95% and 99.7% of the MC
 334 sample are also shown in figure 4 and they give a visual estimation of how likely are
 335 the observations of the output. It can be observed that the surrogate estimates the
 336 regions that contribute more on the lifetime fatigue and even gives an estimation of
 337 the input region on which the largest damage is to be expected. Additionally the MC
 338 simulation on the surrogate gives an estimation of the PDF for each variable, see fifth
 339 column in figure 4.

340 The obtained distribution of power shows a similar behaviour to the operational
 341 data of wind turbines; this shows that one of the main drivers for variability in the
 342 prediction of power below rated is the TIR. Similarly, the thrust coefficient shows large
 343 variability for wind speeds below rated; this large variability can become important
 344 for wake models that use the thrust coefficient to predict the strength of the wake of a
 345 turbine and its impact on other turbines in a wind farm. The fatigue load blade root
 346 and tower top bending moments (BRF, TTT and TTY) show similar dependency on

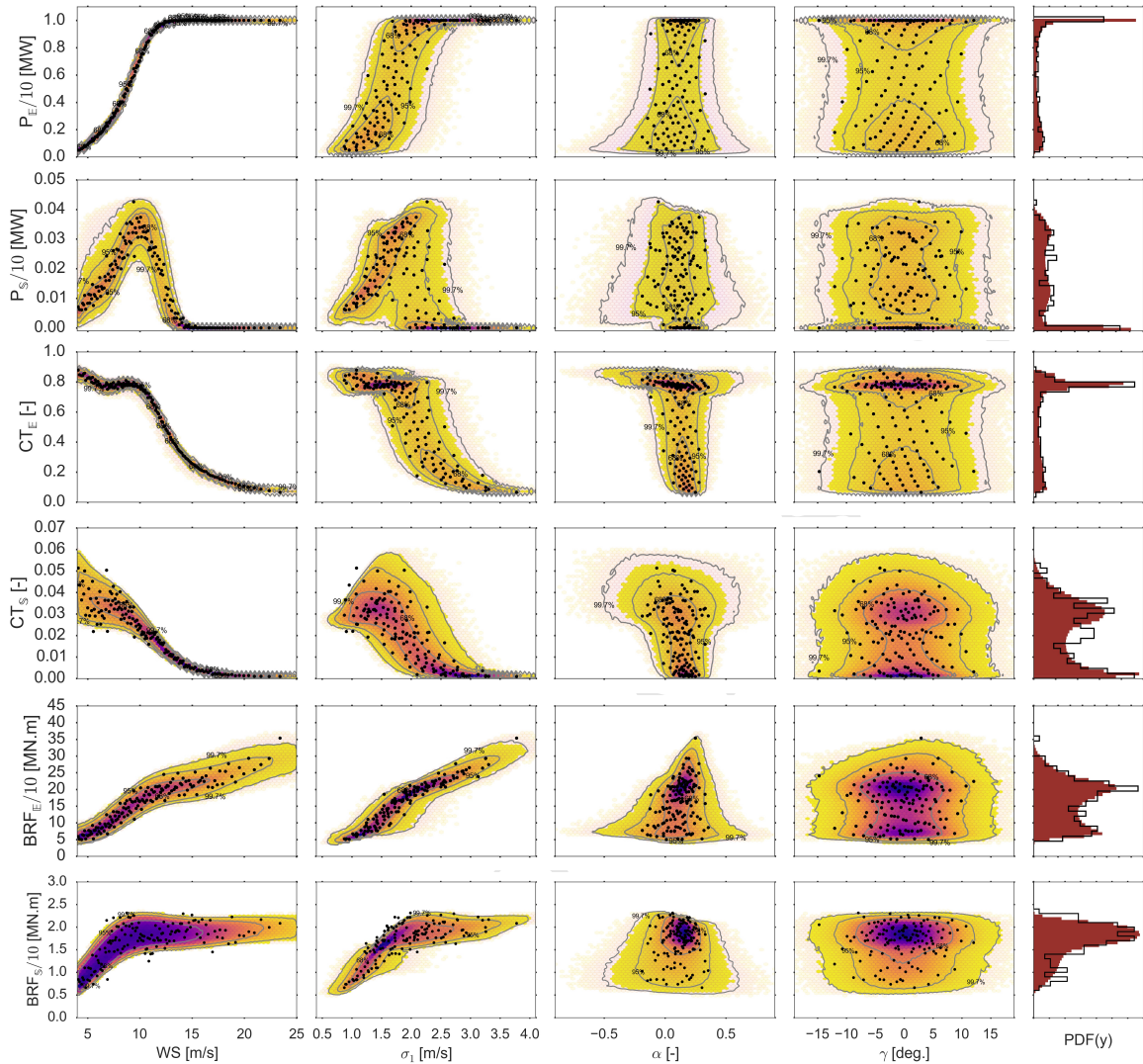


Figure 3: Example of surrogates for mean and std of the output with respect TIR. (Black points) 140 training points. (Histogram colored hex-bins) 80000 MC simulation on the surrogate. (Contour lines) Iso-PDF lines that encircle 68%, 95% and 99.7% of the MC simulation on the surrogate.

347 the four input variables and a similar amount of variability due to TIR; this is because
 348 they are all driven by the streamwise flow field. The fatigue loads tower bottom bending
 349 moments (TBF and TBS) show a different dependency on the input variables, mainly
 350 because they are driven by the thrust and sidewise forces; these two outputs have larger
 351 variability at lower WS which generates both the largest and lowest observations.

352 3.6. Sensitivity analysis

353 The global sensitivity analysis (SA) for the outputs are presented in table 4. The
 354 total effect Sobol indexes are computed using the approximation presented by Saltelli
 355 et al [29]. The total effect Sobol index represents the non-linear influence of the input

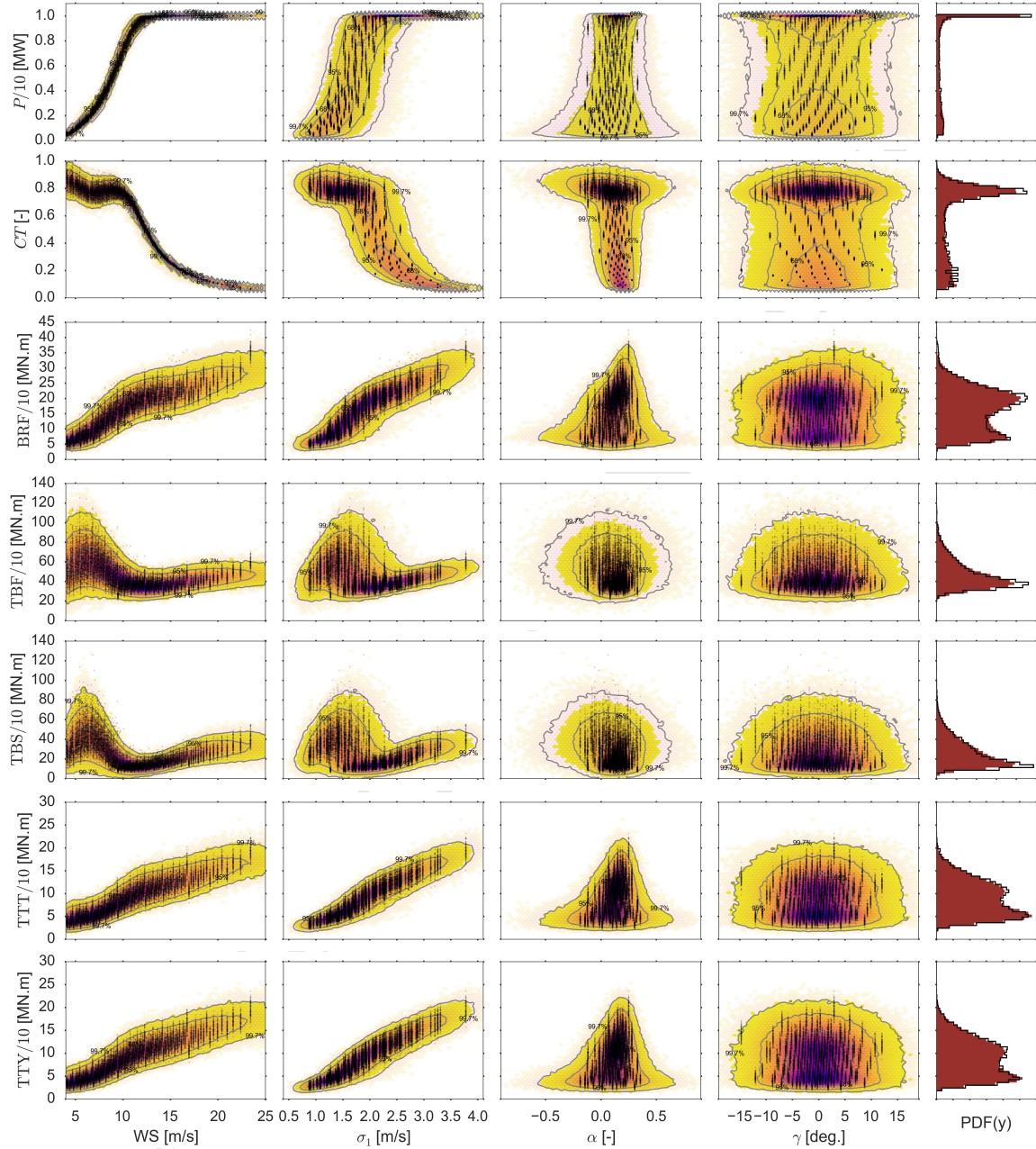


Figure 4: (Black crosses) 10-min HAWC2 simulation for the 140 input sample \times 100 turbulent inflow realizations. (Histogram colored hex-bins) 80000 MC simulation of the surrogate. (Contour lines) Iso-PDF lines that encircle 68%, 95% and 99.7% of the MC simulation on the surrogate.

356 variable in the total variance of the output. Most of the outputs have a large total
 357 Sobol index for the wind speed. WS is clearly the main variable to explain the power
 358 and loads in a wind turbine. The SA shows that the power and thrust coefficient can
 359 be explained almost fully by the WS, since all the terms in the surrogate have WS
 360 dependency.

361 The variance introduced by the turbulent inflow realization is an important com-
 362 ponent for all the outputs, it has a higher influence than σ_1 for most outputs. This
 363 counter intuitive result is due to the large amount of correlation between WS and σ_1 ;
 364 thus a large fraction of the variance of the output generated by σ_1 is already explained
 365 by WS. The shear and yaw have reduced effects over most output variables. The
 366 yaw misalignment has reduced total effect because its assumed distribution is centered
 367 around zero. The shear exponent becomes important only for capturing the fatigue at
 368 the tower top tilt and yaw bending moments (TTT, TTY); while the yaw misalign-
 369 ment becomes important for modeling the fatigue at the tower bottom fore-aft moment
 370 (TBF).

	WS	σ_1	α	γ	TIR
P	1.0	2.4×10^{-4}	3.1×10^{-4}	8.1×10^{-5}	3.1×10^{-3}
	1st	4th	3rd	5th	2nd
CT	9.9×10^{-1}	1.2×10^{-3}	1.3×10^{-3}	6.5×10^{-4}	9.8×10^{-3}
	1st	3rd	4th	5th	2nd
BRF	8.8×10^{-1}	5.6×10^{-2}	1.5×10^{-2}	3.4×10^{-3}	6.7×10^{-2}
	1st	3rd	4th	5th	2nd
TBF	5.9×10^{-1}	2.1×10^{-1}	3.6×10^{-4}	1.0×10^{-3}	3.0×10^{-1}
	1st	3rd	5th	4th	2nd
TBS	7.1×10^{-1}	7.6×10^{-2}	2.1×10^{-3}	2.3×10^{-4}	3.0×10^{-1}
	1st	3rd	5th	4th	2nd
TTT	8.7×10^{-1}	7.1×10^{-2}	3.3×10^{-4}	5.7×10^{-4}	7.7×10^{-2}
	1st	3rd	5th	4th	2nd
TTY	8.7×10^{-1}	6.8×10^{-2}	2.2×10^{-4}	9.6×10^{-4}	7.2×10^{-2}
	1st	3rd	5th	4th	2nd

Table 4: Total influence Sobol index.

371 The sensitivity analysis conditioned on WS for the outputs are presented in table 5.
 372 It can be observed that for power and thrust coefficient the influence of TIR goes from
 373 being the main source of variability at WS below rated to become the least important
 374 for WS above rated; this result summarizes the influence of the pitch controller enforc-
 375 ing the power and limiting the thrust. The effect of TIR in the fatigue loads is more
 376 uniform through all the ranges of operation. Similarly to the global SA, the main
 377 variables required to explain the equivalent fatigue loads are TIR and σ_1 . This is also
 378 true for the power and thrust coefficient for WS below rated.

379 3.7. Convergence

380 A leave-one-out cross-validation (LOO) is done to estimate the distribution of the
 381 prediction error of each surrogate as a function of the number of independent turbulent
 382 seeds per input points used in the surrogate training. A LOO is a cross validation
 383 in which the surrogate is trained leaving one point out. Then, the local statistical

	WS=8 ms ⁻¹				WS=12 ms ⁻¹				WS=16 ms ⁻¹			
	σ_1	α	γ	TIR	σ_1	α	γ	TIR	σ_1	α	γ	TIR
P	1.1 × 10 ⁻¹ 3rd	1.4 × 10 ⁻¹ 2nd	2.8 × 10 ⁻² 4th	7.9 × 10 ⁻¹ 1st	7.8 × 10 ⁻² 2nd	3.7 × 10 ⁻² 3rd	2.5 × 10 ⁻² 4th	9.8 × 10 ⁻¹ 1st	3.0 2nd	1.6 3rd	3.7 1st	9.7 × 10 ⁻¹ 4th
CT	5.1 × 10 ⁻² 3rd	1.1 × 10 ⁻¹ 2nd	3.7 × 10 ⁻² 4th	8.6 × 10 ⁻¹ 1st	2.4 × 10 ⁻¹ 2nd	2.1 × 10 ⁻¹ 3rd	1.5 × 10 ⁻¹ 4th	6.4 × 10 ⁻¹ 1st	6.1 × 10 ⁻¹ 1st	4.3 × 10 ⁻¹ 2nd	3.3 × 10 ⁻¹ 3th	2.0 × 10 ⁻¹ 4th
BRF	4.8 × 10 ⁻¹ 2nd	3.3 × 10 ⁻² 3rd	1.1 × 10 ⁻² 4th	5.0 × 10 ⁻¹ 1st	3.9 × 10 ⁻¹ 2nd	1.0 × 10 ⁻¹ 3rd	9.2 × 10 ⁻³ 4th	5.1 × 10 ⁻¹ 1st	3.5 × 10 ⁻¹ 2nd	1.8 × 10 ⁻¹ 3rd	2.7 × 10 ⁻² 4th	4.6 × 10 ⁻¹ 1st
TBF	3.7 × 10 ⁻¹ 2nd	4.6 × 10 ⁻⁴ 4th	1.9 × 10 ⁻³ 3rd	6.5 × 10 ⁻¹ 1st	5.6 × 10 ⁻¹ 1st	2.1 × 10 ⁻³ 3rd	1.9 × 10 ⁻³ 4th	4.5 × 10 ⁻¹ 2nd	5.2 × 10 ⁻¹ 1st	3.6 × 10 ⁻³ 4th	4.0 × 10 ⁻³ 3rd	4.8 × 10 ⁻¹ 2nd
TBS	1.9 × 10 ⁻¹ 2nd	3.2 × 10 ⁻³ 3rd	6.8 × 10 ⁻⁴ 4th	8.3 × 10 ⁻¹ 1st	2.4 × 10 ⁻¹ 2nd	8.7 × 10 ⁻⁴ 4th	1.7 × 10 ⁻³ 3rd	7.8 × 10 ⁻¹ 1st	2.2 × 10 ⁻¹ 2nd	1.4 × 10 ⁻³ 4th	1.5 × 10 ⁻³ 3rd	7.9 × 10 ⁻¹ 1st
TTT	5.6 × 10 ⁻¹ 1st	2.2 × 10 ⁻³ 3rd	4.0 × 10 ⁻³ 4th	4.5 × 10 ⁻¹ 2nd	4.6 × 10 ⁻¹ 2nd	1.3 × 10 ⁻³ 4th	3.6 × 10 ⁻³ 3rd	5.5 × 10 ⁻¹ 1st	4.6 × 10 ⁻¹ 2nd	2.5 × 10 ⁻³ 4th	3.5 × 10 ⁻³ 3rd	5.4 × 10 ⁻¹ 1st
TTY	5.3 × 10 ⁻¹ 1st	1.9 × 10 ⁻³ 3rd	1.9 × 10 ⁻³ 4th	4.8 × 10 ⁻¹ 2nd	4.6 × 10 ⁻¹ 2nd	5.6 × 10 ⁻⁴ 4th	4.5 × 10 ⁻³ 3rd	5.5 × 10 ⁻¹ 1st	4.7 × 10 ⁻¹ 2nd	1.7 × 10 ⁻³ 4th	1.2 × 10 ⁻² 3rd	5.3 × 10 ⁻¹ 1st

Table 5: Total influence Sobol index at different WS.

384 moments of the output predicted by the surrogates at the missing point are compared
385 against the statistics computed using the surrogate. In this article, the prediction
386 errors are normalized with respect to the maximum scale of the output variable, which
387 means that the errors represent the fraction of the total scale that should be considered
388 as an extra uncertainty due to the inadequacy of the surrogate. The prediction error
389 for the local surrogates are defined as:

$$\begin{aligned}\epsilon_{y\mathbb{E}} &= \frac{y_{\mathbb{E}}(\mathbf{x}_{LO}) - \hat{y}_{\mathbb{E}}(\mathbf{x}_{LO})}{\max(y)} \\ \epsilon_{y\mathbb{S}} &= \frac{y_{\mathbb{S}}(\mathbf{x}_{LO}) - \hat{y}_{\mathbb{S}}(\mathbf{x}_{LO})}{\max(y)}\end{aligned}\quad (14)$$

390 The convergence of the prediction error of the statistical moments is shown in figure
391 5. It can be seen that all the prediction errors tend to be distributed around zero and
392 their standard deviations converge as the number of turbulent inflow realizations per
393 input are increased. The errors converge to the distribution of the errors to the current
394 surrogate. New input points need to be added to the training data set in order to further
395 narrow the converged distribution of surrogate errors. In this figure the outliers are the
396 extreme cases of selecting seeds with similar outputs, therefore, they are those cases
397 that have large errors in the statistical moments. Finally, the converged distribution
398 can be used to estimate the uncertainty in the final prediction of the output as:

$$\hat{y}(\mathbf{x}) \sim \text{Normal}(\hat{y}_{\mathbb{E}}(\mathbf{x}) + \epsilon_{y\mathbb{E}} \max(y), \hat{y}_{\mathbb{S}}(\mathbf{x}) + \epsilon_{y\mathbb{S}} \max(y)) \quad (15)$$

399 where the errors of the surrogates can be sampled from the distribution predicted using
400 LOO cross validation, see figure 5:

$$\epsilon_{y\mathbb{E}} \sim \text{Normal}(\mathbb{E}(\epsilon_{y\mathbb{E}}), \mathbb{S}(\epsilon_{y\mathbb{E}})) \quad \epsilon_{y\mathbb{S}} \sim \text{Normal}(\mathbb{E}(\epsilon_{y\mathbb{S}}), \mathbb{S}(\epsilon_{y\mathbb{S}})) \quad (16)$$

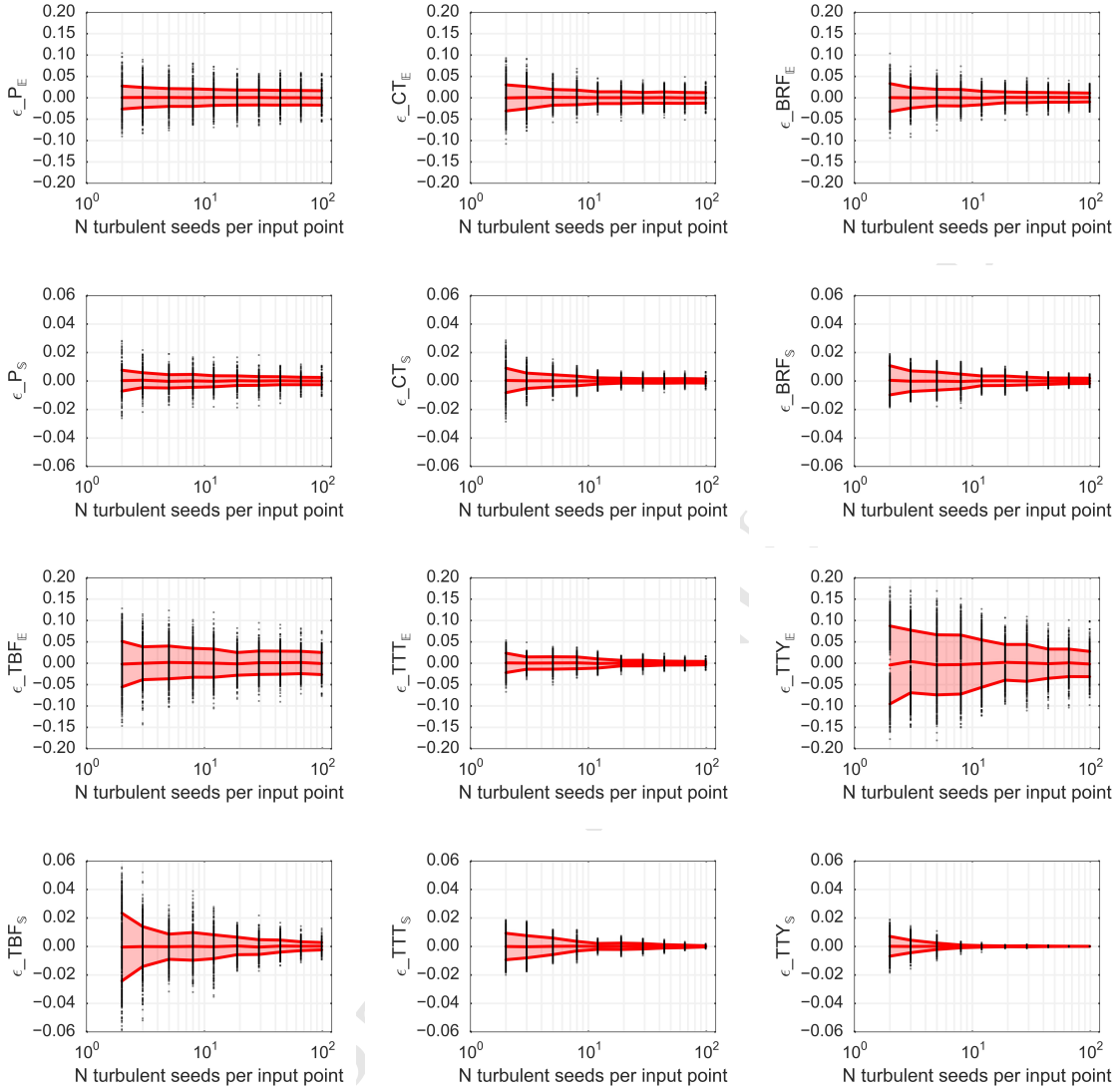


Figure 5: Convergence of the LOO cross-validation prediction error as a function of the number of turbulent seeds per input point used in PCE training. (Pink area) One standard deviation confidence interval around the mean $\mathbb{E}(\epsilon) \pm \mathbb{S}(\epsilon)$.

401 *3.8. Example of using the surrogates for the estimation of the uncertainty in annual*
 402 *energy production and lifetime equivalent fatigue loads*

403 This section presents an example to illustrate the use of the surrogates of the
 404 DTU 10 MW RWT to estimate the uncertainty in the distribution of expected energy
 405 production and of equivalent fatigue loads $\mathbb{E}_{\mathbf{x}}(\mathbf{y})$ in a given period; here the averaging
 406 period is either 1 year or 20 years. In this example a single turbine is planned to operate
 407 in a location from which the uncertainty in the wind resources has been estimated
 408 before hand. This uncertainty can represent the year-to-year variability, the effect of
 409 the long-term correction, uncertainty in the wind resources assessment tool, among

410 other sources of uncertainty. The propagation of uncertainty is done in two steps as
 411 described in figure 6. The inner level predicts the distribution of the turbine outputs
 412 PDF(\mathbf{y}) given a joint distribution of the turbulent inflow parameters PDF(\mathbf{x}); the
 413 inner level returns the expected value of the output to the outer level. In the outer
 414 level the uncertainty in the resources is propagated through the inner level to estimate
 415 the uncertainty of the expected value of each output.

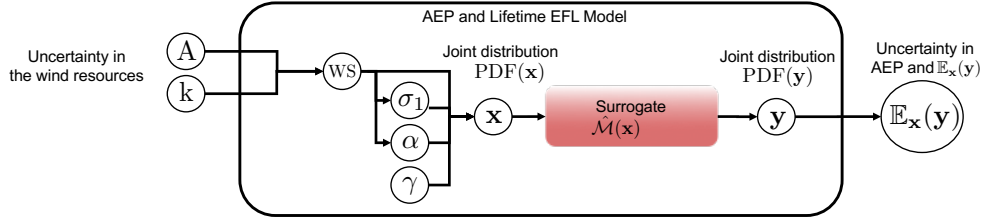


Figure 6: 2 levels of propagation of uncertainty.

416 The distribution of the variability of the wind resources is presented in table 6. The
 417 main difference with the distribution used for training the surrogates is the fact that the
 418 WS follows a Weibull distribution with uncertain shape and scale parameters. This dis-
 419 tribution of the Weibull parameters is used to characterize the variability/uncertainty
 420 in the wind resources. Nevertheless, the conditional distributions of σ_1 , α and γ with
 421 respect WS follow the same dependency described in table 2.

Variable	Distribution	Parameters	
A	Normal	$\mu_A = 9$	$\sigma_A = 0.5$ m/s
k	Normal	$\mu_k = 2$	$\sigma_k = 0.1$
$x_0 = \text{WS}$	Weibull	scale= A	shape= k
$x_1 = \sigma_1$	Lognormal	$\mu_{\sigma_1}(\text{WS})$	$\sigma_{\sigma_1}(\text{WS})$
$x_2 = \alpha$	Normal	$\mu_{\alpha}(\text{WS})$	$\sigma_{\alpha}(\text{WS})$
$x_3 = \gamma$	Normal	$\mu_{\gamma} = 0$	$\sigma_{\gamma} = 5$ deg.

Table 6: Uncertainty in wind resources.

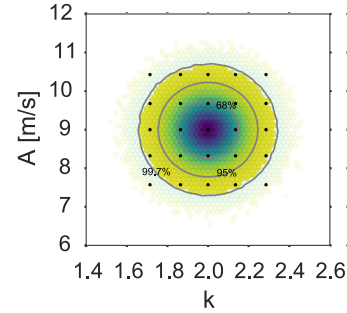


Figure 7: Joint distribution of the Weibull parameters and semi-spectral projection nodes for outer level propagation of uncertainty.

422 The propagation of uncertainty in the outer level is done using both a 1000 MC
 423 sample and a PCE with semi-spectral projection, for which a total of 25 Weibull pa-
 424 rameters nodes are evaluated with their corresponding Gaussian quadrature weights,
 425 see figure 7 and equation 3. Each node or element of the outer level MC sample rep-
 426 represents a realization of the wind resources in a given year. For each of these nodes,
 427 a large inner level sample of the inputs of the surrogate, $\mathbf{x} = [\text{WS}, \sigma_1, \alpha, \gamma]$, is gener-
 428 ated. The size of the inner level MC sample is the number of 10-min cases in a year,
 429 $365 \times 24 \times 6 = 52,560$ cases. The power and EFL are evaluated using the surrogate
 430 and the mean power and mean EFL for a given year are calculated $\mathbb{E}_{\mathbf{x}}(\mathbf{y})$. Note that

431 the definition of the lifetime damage equivalent fatigue load (see eq. 13) requires to
 432 take the average of the individual 10-min EFL to the Wöhler exponent, which trans-
 433 lates in taking a higher order statistical moment: $\mathbb{E}_{\mathbf{x}}(\mathbf{y}^m)$. Each individual surrogate
 434 evaluation has its own realization of the local distribution of the outputs due to the
 435 turbulence inflow realization, see equation 1. Additionally, the effect of the errors of
 436 the surrogate are considered, by sampling the distribution of the errors for each eval-
 437 uation of the outputs, see equation 15. There are no differences in the distributions of
 438 $\mathbb{E}_{\mathbf{x}}(\mathbf{y})$ obtained using the surrogate or the ones obtained including the uncertainty of
 439 the surrogate due to the large sample size of the inner level (52, 560); this means that
 440 the errors of the surrogate cancel out when computing their mean on a given year.

441 A 1000 MC sample of the distribution of one year $\mathbb{E}_{\mathbf{x}}(\mathbf{y})$ is generated using the
 442 PCE of the outer level in order to have an equivalent database of 1000 years as the one
 443 obtained in the outer MC simulation. A bootstrap of the outer level sample is used to
 444 estimate the variation in the expected value during 20 years of operation. This means
 445 that the average of 20 randomly selected years is computed for several realizations of
 446 20 years. The central limit theorem is also used to estimate the distribution of the
 447 average of 20 randomly selected (independent) years. The distributions of the 1 year
 448 and 20 years capacity factor and of lifetime equivalent fatigue loads are presented in
 449 figure 8. It can be observed how the 20-year-averaged distribution has a narrower
 450 distribution, $\sigma_{20yr} = \sigma_{1yr}/\sqrt{20}$. Note that the yearly distribution of average output is
 451 required in order to estimate the uncertainty in the 20-year-averaged output. In this
 452 example coefficient of variations (CoV = σ/μ) of 5.6% for the scale parameter (A) and
 453 5.0% for the shape parameter (k) of the WS Weibull distribution give a coefficient of
 454 variation of 2.4% in AEP and a 9.5% in year-to-year expected power production. The
 455 coefficient of variation in the 20-year damage equivalent BRF is 8.0% while the CoV of
 456 the year-to-year damage equivalent BRF is 35.0%. The CoV for the TBF are 1.0% for
 457 the 20-year damage equivalent load and 4.0% for the year-to-year variation. Note that
 458 this coefficients of variations will be modified if the correlation between the WS and the
 459 other turbulent inflow parameters changes from year to year. It is important to realize
 460 that the distribution for the year-year equivalent damage BRF is skewed due to the
 461 large Wöhler exponent of the composite blades used in this study (12). Nevertheless,
 462 the lifetime equivalent damage BRF converges to a Normal distribution which can be
 463 estimated from the mean and variance of the PCE of the yearly distribution.

464 4. Discussion

465 The present article presents a methodology to implement sparse polynomial sur-
 466 rogates for aeroelastic wind turbine models. PCE are widely used in the uncertainty
 467 quantification field due to their efficiency to compute the statistical properties of the
 468 output and because the sensitivity analysis is obtained without any additional effort.
 469 The main two limitations in the use of PCE for wind energy are: (1) The input at-
 470 mospheric parameters are usually jointly distributed with several layers of dependency
 471 (2) Some of the output have discontinuities and/or are restricted to certain values (e.g.

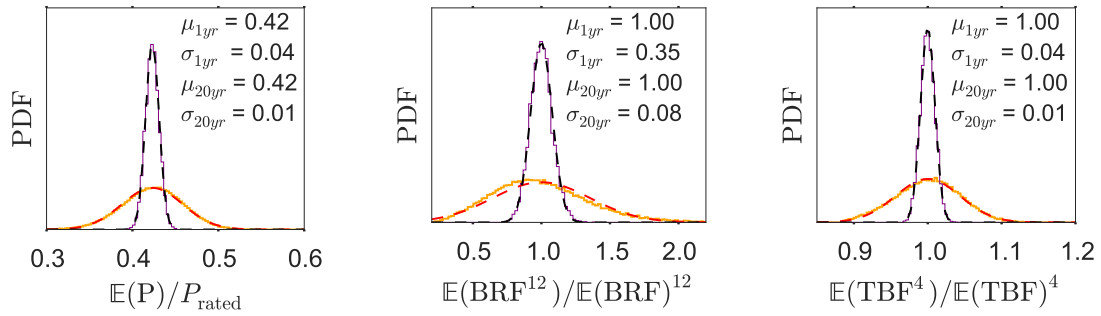


Figure 8: Distribution of the capacity factor and of the expected BRF and TBF equivalent loads. (Red) Normal distribution with the mean and variance predicted with the PCE distribution of the 1 year expected output. (Orange) 1000 MC sample of the 1 year expected output. (Black) Central limit distribution of 20-year-averaged output. (Purple) 1000 Bootstraps of the 20-year-averaged output.

only positive). The present article has shown how to solve these two problems: the implementation of an iso-probabilistic transformation to de-correlate the inputs, and the use of a logistic transformation to implement restrictions on the outputs. The benefits of using the logistic transformation can be seen in figure 3, note that the polynomial surrogates do not present oscillations in the constant regions.

The final surrogate can be used to generate an output sample that covers the full output space, and that will predict the general details of the distributions of the outputs. One of the main limitations of the present surrogates is that the local distribution of the output is assumed to be normal, this is not the case for the operating region close to rated wind speed. Since this assumption only affects the turbulent inflow realization, it is considered to be an acceptable approximation. The local distributions of most outputs are not normal in reality, because the wind turbine controller has different strategies in each operating region, which creates skewness in the local distributions.

The results presented in this article show that there are multiple dependencies between the input variables as well as between inputs and outputs. Such complicated inter-dependencies are difficult to capture when applying other methods such as interpolation or Gaussian processes. For example, advanced interpolation methods such as radial basis functions will not account for the likelihood of an extreme training point and will generate trends that always pass through all the model observations. This behavior penalizes the capacity of the surrogate to generalize and to predict the output in new conditions. The sparse PCE are ideal for this class of problems because the k-fold cross validation is a step inside the training. Additionally, the correlations between the outputs are fully captured when using the presented surrogates; this occurs because each of the outputs has a dependency on the inputs. The full pair plot of the training dataset and the resulting surrogate for all inputs and outputs is presented in the extra material accompanying this article.

The final results presented in figures 4 and 8 show a promising new approach to

499 communicate the performance characteristics of a wind turbine between the turbine
500 manufacturers and project developers. The wind turbine producers normally do not
501 share the detailed structural and aerodynamic model information of their products
502 due to intellectual property concerns. As a result, often the wind project planners
503 and operators do not have the full information about the expected performance of a
504 turbine at the site they are developing. Furthermore, typically there is no model for
505 the uncertainty of the turbine performance. A possible application of the multiple
506 polynomial surrogates of a wind turbine could involve fitting the model by the manu-
507 facturer, and consequent distribution of the surrogate to users and clients. With this
508 approach, project developers could get a useful tool for assessing site feasibility includ-
509 ing uncertainty estimation, while not requiring access to detailed engineering models.
510 Consequently, the use of more refined site assessment can potentially lead to improved
511 overall estimation of levelized cost of energy and its uncertainty.

512 Obtaining the $PDF(P)$ and $PDF(EFL)$ is useful as they can be used for uncertainty
513 estimation of the levelized cost of energy on a yearly basis. The surrogates can be
514 evaluated on a long time series of the local wind resources (in multiple variables) such
515 as the ones predicted by Weather Research and Forecasting (WRF) models without
516 considerable extra computational effort. The power surrogate can then predict the
517 annual variation of energy production while the EFL can be used to estimate the
518 operation and maintenance costs. Such a probabilistic output can be the input to a
519 decision support tool.

520 A surrogate of the DTU 10 MW RWT within a 4-dimensional turbulent inflow
521 parameter space can be built using only 140 input cases (with multiple turbulent
522 inflow realizations per case) and can be used to predict the distribution of the power,
523 thrust coefficient and equivalent fatigue loads on the turbine. In contrast, traditional
524 approaches require in the order of 20^4 gridsearch/interpolation (full factorial design
525 with 20 points per dimension) or $10^5 - 10^6$ MC sample of the inputs with variance
526 reduction [22]. Furthermore, the present approach enables to build an uncertainty
527 model around the 10 minutes performance of the turbine that captures the effect of
528 the turbulent inflow realization.

529 The combined PCE surrogate approach can also be used to improve traditional
530 designs in which a conservative scenario for shear and turbulence intensity is consid-
531 ered. The fast evaluation of the joint probability distributions for loads based on the
532 surrogate model opens possibilities for performing structural reliability analysis and
533 probability based design.

534 5. Conclusions

535 In the present study, a polynomial surrogate model of wind turbine fatigue loads
536 and energy output was defined and demonstrated for the DTU 10 MW reference wind
537 turbine. Using only 140 input cases was found to be sufficient for building a surrogate
538 of the DTU 10MW model within a 4-dimensional turbulent inflow parameter space.
539 The presented approach was demonstrated as an efficient alternative of the traditional

540 techniques for characterizing the global behavior of an aeroelastic wind turbine model
541 under multiple uncertain turbulent inflow parameters.

542 The surrogate has enabled us to perform a global sensitivity analysis on the DTU 10
543 MW turbine. This study showed that the hub height wind speed is the most important
544 variable to predict the power of the turbine, followed by the turbulent inflow realization
545 (TIR); this is a consequence of the correlation between turbulence intensity, shear and
546 hub height wind speed. The turbulence intensity is of similar importance as the TIR in
547 the prediction of blade root flapwise (BRF), and tower top tilt (TTT) and yaw (TTY)
548 equivalent fatigue loads.

549 The surrogate can be used in a two-level propagation of uncertainty example. In
550 the example presented in this article the year-to-year variability in the shape and scale
551 parameters of the hub height wind speed Weibull distribution are propagated into a
552 variation of AEP and of lifetime equivalent fatigue loads. Coefficient of variations of
553 5.6% for the scale and of 5% for the shape parameters give a coefficient of variation of
554 2.4% in AEP, of 1.8% in lifetime $\mathbb{E}(BRF)$ and of 0.5% in lifetime $\mathbb{E}(TBF)$.

555 Finally, the methodology presented in this article can be used in other applica-
556 tions in which there are fields which might take multiple realizations such as marine
557 structures (wave and current fields), offshore structures (wave and wind fields) or soil-
558 foundation structures (soil properties fields) among others.

559 6. Acknowledgments

560 This work was supported by the International Collaborative Energy Technology
561 R&D Program of the Korea Institute of Energy Technology Evaluation and Planning
562 (KETEP), granted financial resource from the Ministry of Trade, Industry & Energy,
563 Republic of Korea. (No. 20138520021140). The authors will like to thank Michael
564 McWilliam for the suggestion of the use of logistic transformations to enforce strict
565 restrictions to the polynomial surrogates.

566 References

- 567 [1] I. E. Commission, et al., Iec 61400-1: Wind turbines part 1: Design requirements,
568 International Electrotechnical Commission.
- 569 [2] P. A. Graf, G. Stewart, M. Lackner, K. Dykes, P. Veers, High-throughput computation
570 and the applicability of monte carlo integration in fatigue load estimation of floating
571 offshore wind turbines, *Wind Energy*.
- 572 [3] H. S. Toft, L. Svenningsen, W. Moser, J. D. Sørensen, M. L. Thøgersen, Assessment
573 of wind turbine structural integrity using response surface methodology, *Engineering*
574 *Structures* 106 (2016) 471–483.
- 575 [4] I. Abdallah, A. Natarajan, J. D. Sørensen, Influence of the control system on wind
576 turbine loads during power production in extreme turbulence: Structural reliability,
577 *Renewable Energy* 87 (2016) 464–477.

- 578 [5] A. Clifton, L. Kilcher, J. Lundquist, P. Fleming, Using machine learning to predict wind
579 turbine power output, *Environmental research letters* 8 (2) (2013) 024009.
- 580 [6] A. Clifton, M. Daniels, M. Lehning, Effect of winds in a mountain pass on turbine
581 performance, *Wind Energy* 17 (10) (2014) 1543–1562.
- 582 [7] C. Soize, R. Ghanem, Physical systems with random uncertainties: chaos representations
583 with arbitrary probability measure, *SIAM Journal on Scientific Computing* 26 (2) (2004)
584 395–410.
- 585 [8] O. Le Maître, O. Knio, H. Najm, R. Ghanem, Uncertainty propagation using wiener-
586 haar expansions, *Journal of computational Physics* 197 (1) (2004) 28–57.
- 587 [9] S.-K. Choi, R. V. Grandhi, R. A. Canfield, C. L. Pettit, Polynomial chaos expansion
588 with latin hypercube sampling for estimating response variability, *AIAA journal* 42 (6)
589 (2004) 1191–1198.
- 590 [10] M. Berveiller, B. Sudret, M. Lemaire, Stochastic finite element: a non intrusive approach
591 by regression, *European Journal of Computational Mechanics/Revue Européenne de*
592 *Mécanique Numérique* 15 (1-3) (2006) 81–92.
- 593 [11] D. Xiu, J. S. Hesthaven, High-order collocation methods for differential equations with
594 random inputs, *SIAM Journal on Scientific Computing* 27 (3) (2005) 1118–1139.
- 595 [12] G. Blatman, B. Sudret, Adaptive sparse polynomial chaos expansion based on least angle
596 regression, *Journal of Computational Physics* 230 (6) (2011) 2345–2367.
- 597 [13] F. Pedregosa, G. Varoquaux, A. Gramfort, V. Michel, B. Thirion, O. Grisel, M. Blondel,
598 P. Prettenhofer, R. Weiss, V. Dubourg, et al., Scikit-learn: Machine learning in python,
599 *The Journal of Machine Learning Research* 12 (2011) 2825–2830.
- 600 [14] R. Tibshirani, Regression shrinkage and selection via the lasso, *Journal of the Royal*
601 *Statistical Society. Series B (Methodological)* (1996) 267–288.
- 602 [15] P. Moriarty, Database for validation of design load extrapolation techniques, *Wind En-*
603 *ergy* 11 (6) (2008) 559.
- 604 [16] A. Natarajan, D. R. Verelst, Outlier robustness for wind turbine extrapolated extreme
605 loads, *Wind Energy* 15 (5) (2012) 679–697.
- 606 [17] C. Tibaldi, L. C. Henriksen, C. Bak, Investigation of the dependency of wind turbine
607 loads on the simulation time, in: *European Wind Energy Conference & Exhibition 2014*,
608 2014.
- 609 [18] C. Bak, R. Bitsche, A. Yde, T. Kim, M. H. Hansen, F. Zahle, M. Gaunaa, J. P. A. A.
610 Blasques, M. Døssing, J.-J. Wedel Heinen, et al., Light rotor: The 10-mw reference wind
611 turbine, in: *EWEA 2012-European Wind Energy Conference & Exhibition*, 2012.
- 612 [19] M. Rosenblatt, Remarks on a multivariate transformation, *The annals of mathematical*
613 *statistics* 23 (3) (1952) 470–472.

- 614 [20] P. Y. Simard, Y. A. LeCun, J. S. Denker, B. Victorri, Transformation invariance in pat-
615 tern recognition tangent distance and tangent propagation, in: *Neural networks: tricks*
616 *of the trade*, Springer, 1998, pp. 239–274.
- 617 [21] W. Gautschi, Algorithm 726: Orthpol—a package of routines for generating orthogo-
618 nal polynomials and gauss-type quadrature rules, *ACM Transactions on Mathematical*
619 *Software (TOMS)* 20 (1) (1994) 21–62.
- 620 [22] N. Dimitrov, A. Natarajan, M. Kelly, Model of wind shear conditional on turbulence
621 and its impact on wind turbine loads, *Wind Energy* 18 (11) (2015) 1917–1931.
- 622 [23] J. Feinberg, H. P. Langtangen, Chaospy: An open source tool for designing methods of
623 uncertainty quantification, *Journal of Computational Science* 11 (2015) 46–57.
- 624 [24] M. D. McKay, R. J. Beckman, W. J. Conover, A comparison of three methods for
625 selecting values of input variables in the analysis of output from a computer code, *Tech-*
626 *nometrics* 42 (1) (2000) 55–61.
- 627 [25] I. M. Sobol’, On the distribution of points in a cube and the approximate evaluation
628 of integrals, *Zhurnal Vychislitel’noi Matematiki i Matematicheskoi Fiziki* 7 (4) (1967)
629 784–802.
- 630 [26] J. M. Hammersley, Monte carlo methods for solving multivariable problems, *Annals of*
631 *the New York Academy of Sciences* 86 (3) (1960) 844–874.
- 632 [27] I. M. Sobol, Global sensitivity indices for nonlinear mathematical models and their monte
633 carlo estimates, *Mathematics and computers in simulation* 55 (1) (2001) 271–280.
- 634 [28] S. E. Maxwell, H. D. Delaney, *Designing experiments and analyzing data: A model*
635 *comparison perspective*, Vol. 1, Psychology Press, 2004.
- 636 [29] A. Saltelli, P. Annoni, I. Azzini, F. Campolongo, M. Ratto, S. Tarantola, Variance based
637 sensitivity analysis of model output. design and estimator for the total sensitivity index,
638 *Computer Physics Communications* 181 (2) (2010) 259–270.
- 639 [30] B. Sudret, Global sensitivity analysis using polynomial chaos expansions, *Reliability*
640 *Engineering & System Safety* 93 (7) (2008) 964–979.
- 641 [31] M. S. Eldred, A. A. Giunta, B. G. van Bloemen Waanders, S. F. Wojtkiewicz, W. E.
642 Hart, M. P. Alleva, DAKOTA, a multilevel parallel object-oriented framework for design
643 optimization, parameter estimation, uncertainty quantification, and sensitivity analysis:
644 Version 4.1 reference manual, Citeseer, 2007.
- 645 [32] S. Marelli, B. Sudret, UQLab: a framework for uncertainty quantification in MATLAB,
646 ETH-Zürich, 2014.
- 647 [33] G. Andrianov, S. Burriel, S. Cambier, A. Dutfoy, I. Dutka-Malen, E. De Rocquigny,
648 B. Sudret, P. Benjamin, R. Lebrun, F. Mangeant, et al., Open turns, an open source
649 initiative to treat uncertainties, risks n statistics in a structured industrial approach, in:
650 *Proceedings of ESREL*, 2007.

- 651 [34] T. J. Larsen, A. M. Hansen, How 2 HAWC2, the user's manual, Risø National Labora-
652 tory, 2007.
- 653 [35] J. Mann, Wind field simulation, Probabilistic Engineering Mechanics 13 (4) (1998) 269
654 – 282.
- 655 [36] M. A. Miner, et al., Cumulative damage in fatigue, Journal of applied mechanics 12 (3)
656 (1945) 159–164.
- 657 [37] S. Hosder, R. W. Walters, M. Balch, Efficient sampling for non-intrusive polynomial
658 chaos applications with multiple uncertain input variables, in: Proceedings of the 48th
659 AIAA/ASME/ASCE/AHS/ASC Structures, Structural Dynamics and Materials Con-
660 ference, AIAA paper, Vol. 1939, 2007.

Highlights

- Sparse polynomials are proposed as surrogates of an aeroelastic wind turbine model.
- The surrogates can be used to predict the distribution of the 10-min mean power and equivalent fatigue loads under realistic atmospheric conditions.
- The surrogates are used in a two-level uncertainty propagation scenario to estimate the uncertainty in annual energy production and in lifetime equivalent fatigue loads.